A Bidirectional DC–DC Converter for Fuel Cell Electric Vehicle Driving System

Huang-Jen Chiu, *Member, IEEE*, and Li-Wei Lin

***Abstract*—This paper presents a power converter for a fuel cell electric vehicle driving system. A new bidirectional, isolated topology is proposed in consideration of the differing fuel cell characteristics from traditional chemical-power battery and safety requirements. The studied converter has the advantages of high efficiency, simple circuit, and low cost. The detailed design and operating principles are analyzed and described. The simulation and experimental waveforms for the proposed converter are shown to verify its feasibility.**

***Index Terms*—Bidirectional dc–dc converter, electric vehicle, fuel cell.**

I. Introduction

In RECENT years, growing concerns about environmental issues have demanded more energy efficient nonpolluting vehicles. The rapid advances in fuel cell technology and power electronics have enabled the significant developments in fuel cell powered electric vehicles. The fuel cells have numerous advantages such as high density current output ability, clean electricity generation, and high efficiency operation [1]–[5]. However, the fuel cell characteristics are different from that of the traditional chemical-powered battery. The fuel cell output voltage drops quickly when first connected with a load and gradually decreases as the output current rises. The fuel cell also lacks energy storage capability. Therefore, in electric vehicle applications, an auxiliary energy storage device (i.e., lead-acid battery) is always needed for a cold start and to absorb the regenerated energy fed back by the electric machine. In addition, a dc–dc converter is also needed to draw power from the auxiliary battery to boost the high-voltage bus during vehicle starting. Until the fuel cell voltage rises to a level high enough to hold the high-voltage bus, the excess load from the battery will be released. The regenerated braking energy can also be fed back and stored in the battery using the dc–dc converter. A full-bridge bidirectional dc–dc converter, shown in Fig. 1, is considered one of the best choices for these applications [6]. However, this system has a complicated configuration, high cost, and large size. Several half-bridge based topologies have been published in the literature to reduce the device count and increase efficiency [7]–[10]. A voltage imbalance exists between the two split capacitors, thus an additional control circuit to eliminate the voltage imbalance problem is required. In this paper, a new bidirectional dc–dc converter is presented. The proposed system has the advantages of high efficiency, simple circuit and low cost. Isolating the low- and high-voltage sides satisfies the safety requirements. In the following sections, the design and operating principles will be discussed in detail. Spice simulations are given to confirm the theoretical analysis. A laboratory prototype was implemented and tested to show the performance.

Manuscript received December 8, 2004; revised July 22, 2005. This work was supported by the National Science Council of Taiwan, R. O. C. under Grant NSC 94-2622-E-033-009-CC3. Recommended by Associate Editor A. von Jouanne.

The authors are with the Department of Electrical Engineering, Chung-Yuan Christian University, Chung-Li 32023, Taiwan, R.O.C. (e-mail: hjchiu@dec.ee.cycu.edu.tw).

Digital Object Identifier 10.1109/TPEL.2006.876863

II. Circuit Operation

The circuit topology of the proposed bidirectional isolated converter is shown in Fig. 2. According to the power flow directions, there are two operation modes for the proposed converter. When power flows from the low-voltage side (LVS) to the high-voltage side (HVS), the circuit operates in boost mode to draw energy from the battery. In the other power flow direction, the circuit operates in buck mode to recharge the battery from the high-voltage dc bus. Based on the symbols and signal polarities introduced in Fig. 2, the theoretical waveforms of the two operation modes are shown in Fig. 3(a) and (b), respectively.

A. Boost Mode (Discharging Mode) Operation

When the dc bus voltage in the HVS is not at the desired high level, such as during a cold start, the power drawn from the low-voltage battery flows into the high-voltage dc bus. During this mode, the proposed converter is operated as a current-fed circuit to boost the HVS bus voltage. The LVS switches Q1 and Q2 operate at asymmetrical duty ratios δ and $1-\delta$ which require a short overlapping conduction interval. Referring to the equivalent circuits for the boost mode operation in Fig. 4, the detailed operating principle can be explained as follows.

Stage 1 (t0–t1): At t0, the LVS switch Q2 is turned off and the HVS switch Q3 is turned on. The current from the inductor L_2 flows through Q1 and the transformer LVS winding, closing the loop via the battery. Therefore, the transformer LVS winding carries only I_{L2}. The voltage amplitude across the transformer HVS winding, V_2 can be clamped to the dc voltage, V_{A} on the series blocking capacitor C_{S} with negative polarity while the diode Da conducts. Thus, the voltage across the transformer LVS winding, V_1 is clamped to $(-V_{\mathrm{A}}/n)$. The "n" is the transformer turn ratio. The current I_{L2} increases linearly while I_{L1} decreases linearly. Because the battery current, I_{Bat}, is the sum of the two inductor currents, the ripple currents cancel each other to produce relatively ripple-free dc current that is desirable for the low-voltage battery.

Stage 2 (t1–t2): At t1, the LVS switch Q2 is turned on and the HVS switch Q3 is turned off. During this interval, the switches Q1 and Q2 are on simultaneously. The voltage across L_2 also becomes negative and its' amplitude equals the battery voltage. The inductance current, I_{L2} decreases linearly like the current, I_{L1}. The voltage across the transformer winding become zero

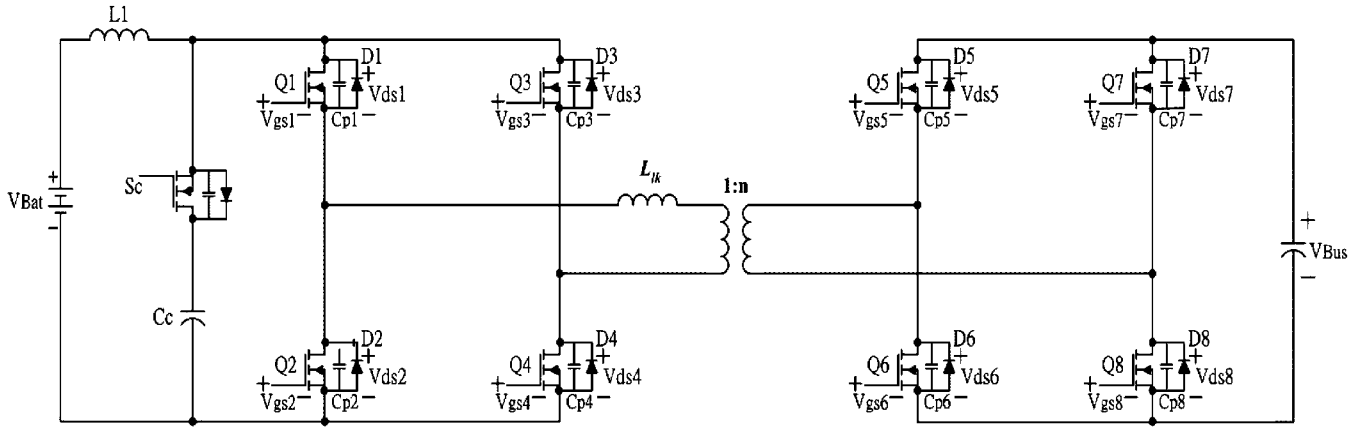

Fig. 1. Conventional full-bridge bidirectional dc–dc converter.

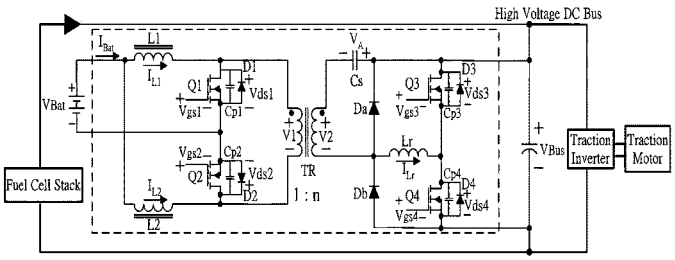

Fig. 2. Proposed isolated bidirectional dc–dc converter.

and the diode Da is reverse-biased. The voltage on the series blocking capacitor, $V_{\rm A}$ will force the inductance current $I_{\rm Lr}$ to change its direction at $t2$.

Stage 3 (t2–t3): The inductor $L_{\rm r}$ resonates with $C_{\rm p3}$ and $C_{\rm p4}$ during this interval. The voltage $V_{\rm ds4}$ across the HVS switch, Q4 continues to decrease to zero at t3.

Stage 4 (t3–t4): At t3, the inductor currents $I_{\rm Lr}$ starts to flow through the body diode D4. As long as the switch Q4 is turned on at t4, zero-voltage switching can be assured.

Stage 5 (t4–t5): At t4, the LVS switch Q1 is turned off and the HVS switch Q4 is turned on. The current from the inductor L_1 flows through Q2 and the transformer LVS winding, closing the loop via the battery. Therefore, the transformer LVS winding carries only $I_{\rm L1}$. The voltage amplitude across the transformer HVS winding, V_2 can be clamped to $(V_{\rm Bus} - V_{\rm A})$ while the diode Db conducts. Thus, the voltage across the transformer LVS winding, V_1 is clamped to $(V_{\rm Bus} - V_{\rm A})$/n. The current $I_{\rm L1}$ increases linearly while $I_{\rm L2}$ decreases linearly. The ripple currents on two inductors cancel each other to produce relatively ripple-free dc current for the low-voltage battery.

Stage 6 (t5–t6): At t5, the LVS switch Q1 is turned on and the HVS switch Q4 is turned off. During this interval, the switches Q1 and Q2 are simultaneously on. The voltage across L_1 also becomes negative and its' amplitude equals the battery voltage. The inductance current, $I_{\rm L1}$ decreases linearly like the current, $I_{\rm L2}$. The voltage across the transformer winding become zero and the diode Db is reverse-biased. The voltage across the inductor Lr, $(V_{\rm Bus} - V_{\rm A})$ will force the inductance current $I_{\rm Lr}$ to change its direction at $t6$.

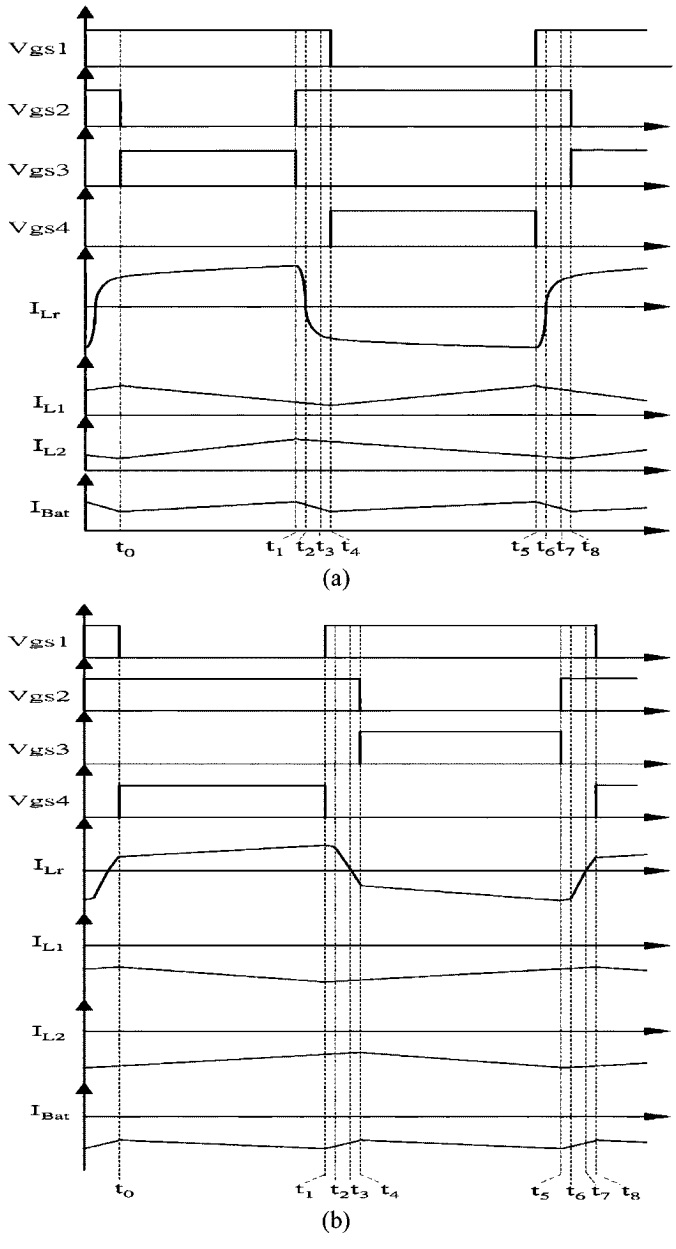

Fig. 3. Theoretical waveforms under (a) boost and (b) buck mode operations.

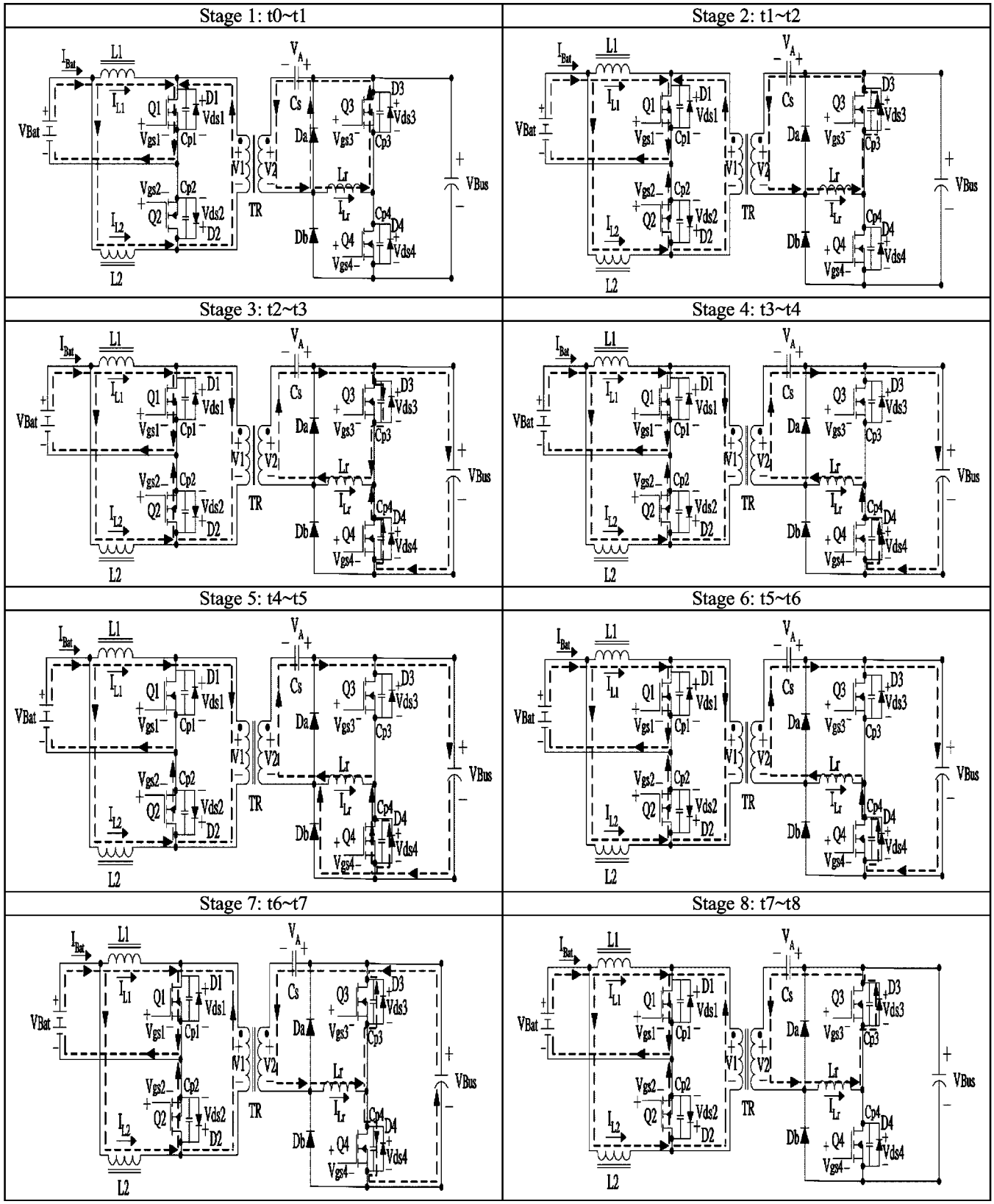

Fig. 4. Equivalent circuits for boost mode operation.

Stage 7 (t6–t7): The inductor $L_{\rm r}$ resonates with $C_{\rm p3}$ and $C_{\rm p4}$ during this interval. The voltage $V_{\rm ds3}$ across the HVS switch, Q3 continues to decrease to zero at $t7$.

Stage 8 (t7–t8): At $t7$, the inductor currents $I_{\rm Lr}$ starts to flow through the body diode $D3$. As long as the switch Q3 is turned on at $t8$, zero-voltage switching can be assured. The circuit will

then proceed back to stage 1 after completing one operating cycle T_s.

Based on the above analysis, the voltage and current stresses of the LVS switches can be found

$$V_{Q1} = V_{\rm Bat}/(1-\delta) \tag{1}$$
$$V_{Q2} = V_{\rm Bat}/\delta \tag{2}$$
$$I_{Q1(\rm mean)} = \delta I_{\rm Bat} \tag{3}$$
$$I_{Q2(\rm mean)} = (1-\delta) I_{\rm Bat}. \tag{4}$$

Although the LVS switches subject to higher voltage stress, this is an advantage because the battery voltage is low. Because the overlapping interval for the LVS switches Q1 and Q2 is very short, the LVS transformer current flows through only one LVS switch at most time. Thus, the conduction losses for Q1 and Q2 can be greatly reduced to improve the conversion efficiency. Moreover, the LVS circuit produces a relatively ripple-free battery current that is desirable for the low voltage battery. Assuming that the capacitors $C_{\rm s}$ and $C_{\rm o}$ are large enough, the voltage ripples on them are negligible. The series blocking capacitor $C_{\rm s}$ will be charged so that the volt-second integral across the transformer primary winding is maintained. Thus, the voltage $V_{\rm A}$ across the series blocking capacitor can be expressed as (5). The tolerable droop in the capacitor voltage is about 20%, so the required capacitor magnitude can be calculated simply as

$$V_A = \frac{nV_{\rm Bat}}{\delta} \tag{5}$$
$$C_s = \frac{\delta(1-\delta)T_s I_{\rm Bat}}{0.2nV_A}. \tag{6}$$

The voltage transfer ratio $M_{\rm boost}$ for the boost mode operation for the proposed dc–dc converter can be derived from the volt-second balance condition across the inductors L_1 or L_2 and represented by (7). The current stresses of the inductor windings can be also determined as (8) and (9). The inductances of the power inductors L_1 and L_2 can be determined for their given peak-to-peak current ripples, ΔI_1 and ΔI_2 as

$$M_{\rm boost} = \frac{V_{\rm Bus}}{V_{\rm Bat}} = \frac{n}{\delta(1-\delta)}, \tag{7}$$
$$I_{\rm L1} = \delta I_{\rm Bat} \tag{8}$$
$$I_{L2} = (1-\delta) I_{\rm Bat} \tag{9}$$
$$L_1 = \frac{\delta V_{\rm Bat} T_s}{\Delta I_1} = \frac{V_{\rm Bat} T_s}{0.01\lambda(\%) I_{\rm Bat}} \tag{10}$$
$$L_2 = \frac{(1-\delta) V_{\rm Bat} T_s}{\Delta I_2} = \frac{V_{\rm Bat} T_s}{0.01\lambda(\%) I_{\rm Bat}} \tag{11}$$

where $\lambda(\%)$ is the ripple percentage of the inductor currents, $I_{\rm L1}$ and $I_{\rm L2}$.

B. Buck Mode (Charging Mode) Operation

Different from the traditional electric vehicle driving system, the fuel cell powered system needs an additional energy storage device to absorb the feedback power from the electric machine. This energy storage device may be a lead-acid battery as shown in Fig. 2. The proposed circuit works in buck mode to recharge the battery from high-voltage dc bus. During this mode, the proposed converter is operated as an asymmetrical half bridge circuit with synchronous rectification current doubler to recharge the battery from high-voltage dc bus. The HVS switches Q3 and Q4 operate at asymmetrical duty ratios δ and $1-\delta$ which require short and well-defined dead time between the conduction intervals. Referring to the equivalent circuits in Fig. 5, the detailed operating principle of this mode can be explained as follows.

Stage 1(t0–t1): At $t0$, the HVS switch Q4 and the LVS switch Q2 stay on. The inductance current $I_{\rm Lr}$ is equal to $-I_{\rm L1}/n$. The current from the inductor L_1 flows through Q2 and the transformer LVS winding, closing the loop via the battery. Therefore, the transformer LVS winding carries only $-I_{\rm L1}$. The current $-I_{\rm L1}$ increases linearly while $-I_{\rm L2}$ decreases linearly. Since the recharging current, $-I_{\rm Bat}$, is the sum of the two inductor currents, the ripple currents cancel each other to produce relatively ripple-free dc current that is desirable for the low-voltage battery.

Stage 2 (t1–t2): At t1, the LVS switch Q1 is turned on and the HVS switch Q4 is turned off. During this interval, the switches Q1 and Q2 are simultaneously on. The recharging current, $-I_{\rm Bat}$, freewheels through both the switches, Q1 and Q2. The voltage across L_1 also becomes negative and equals the battery voltage. Therefore, the inductance current $-I_{\rm L1}$ decreases linearly like the current $-I_{\rm L2}$. The voltage across the transformer winding becomes zero, the inductor $L_{\rm r}$ resonates with $C_{\rm p3}$ and $C_{\rm p4}$. The voltage $V_{\rm ds3}$ across the switch, Q3 continues to decrease to zero at t2.

Stage 3 (t2–t3): At $t2$, the currents $I_{\rm Lr}$ starts to flow through the body diode D3. As long as the HVS switch Q3 is turned on before the inductor current changes its direction at t3, zero-voltage switching can be assured.

Stage 4 (t3–t4): While the HVS switch, Q3 is zero-voltage turned on, the LVS switch, Q2 is turned off. The resonance caused by inductor $L_{\rm r}$ and the stray transformer winding capacitor could be clamped while the diode, Da is conducted. At $t4$, Da is released because the inductance current $-I_{\rm Lr}$ stays at $-I_{\rm L2}/n$. The stages 5–8 are similar to stages 1–4, respectively. The circuit will then proceed back to stage 1 after completing one operating cycle $T_{\rm s}$.

While the LVS switches, Q1 and Q2, share unequal voltage and current stresses, the HVS switches, Q3 and Q4, share equal voltage stresses as (12). Then the current stresses of the HVS switches can be found as

$$V_{Q3} = V_{Q4} = V_{\rm Bus}, \tag{12}$$
$$I_{Q3} = \frac{(1-\delta)|I_{\rm Bat}|}{n} \tag{13}$$
$$I_{Q4} = \frac{\delta|I_{\rm Bat}|}{n}. \tag{14}$$

III. Design Considerations for Key Components

To verify the feasibility of the proposed scheme, a 2-kW laboratory prototype operated at 20 kHz was built. The simulation and experimental results will be shown and discussed in the next section. The LVS of the design example was connected to a 12-V lead-acid battery whose terminal voltage could swing from 10–15 V. The nominal voltage on the HVS dc bus was designed to 300 V, with an operating range from 150–400 V. The design considerations for the key components in the example will be discussed in detail as follows.

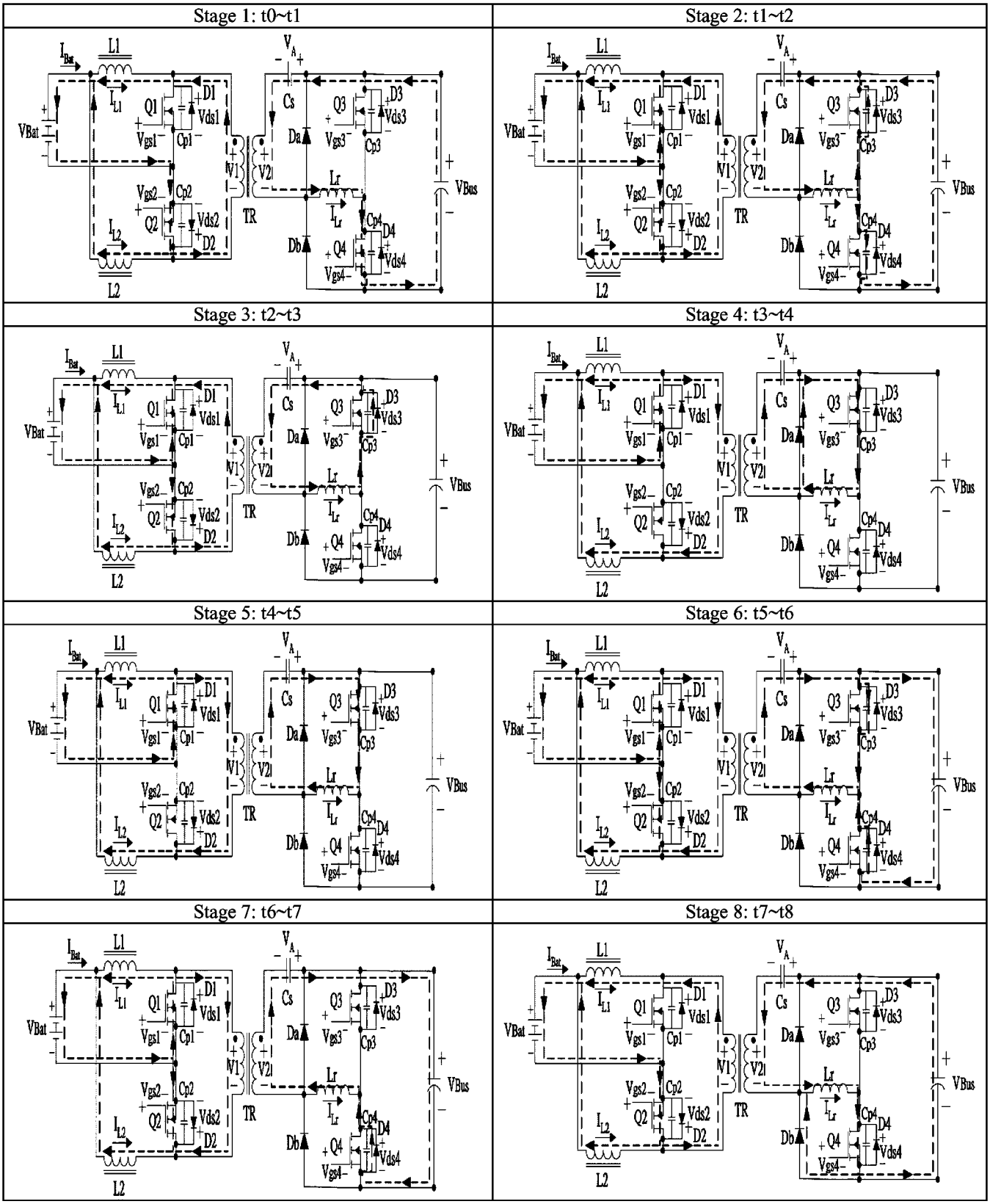

Fig. 5. Equivalent circuits for buck mode operation.

A. Power Switches

The power switch voltage and current ratings are very important converter design topics. When the duty ratio δ is chosen in the operating range of from 0.2 to 0.5, the LVS device rating can be calculated by using (1)–(4) as follows:

$$V_{Q1} = \frac{V_{\mathrm{Bat(max)}}}{1-\delta_{\max}} = 30\ \mathrm{V} \tag{15}$$

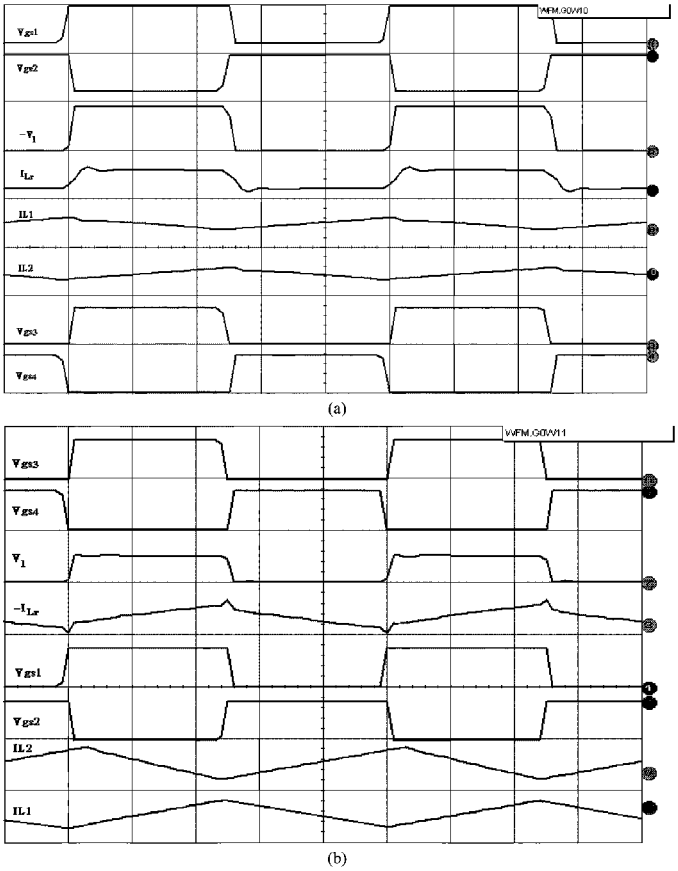

Fig. 6. Simulation results for (a) boost and (b) buck mode operations.

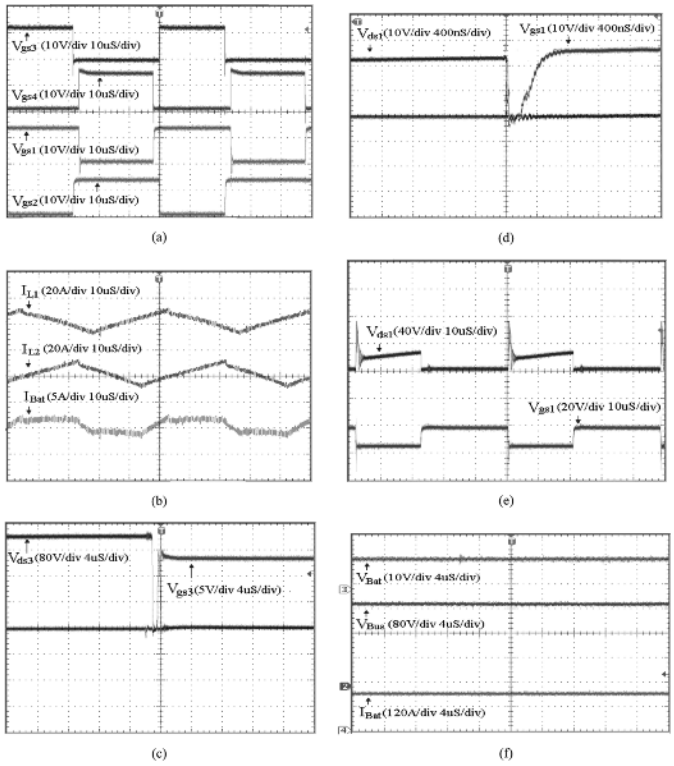

Fig. 7. Experimental results for boost mode operations for the laboratory prototype.

$$V_{Q2} = \frac{V_{\mathrm{Bat(max)}}}{\delta_{\min}} = 75\ \mathrm{V} \tag{16}$$

$$I_{Q1(\mathrm{mean})} = \delta_{\max} I_{\mathrm{Bat(max)}} = 100\ \mathrm{A} \tag{17}$$

$$I_{Q2(\mathrm{mean})} = (1-\delta_{\min}) I_{\mathrm{Bat(max)}} = 160\ \mathrm{A}. \tag{18}$$

Based on (7), the turn-ratio selection of transformer can be calculated as (19). The HVS device ratings can then be calculated using (12)–(14) as follows:

$$n = \frac{V_{\mathrm{Bus}}}{V_{\mathrm{Bat(min)}}}\delta(1-\delta) = 10 \tag{19}$$

$$V_{Q3} = V_{Q4} = V_{\mathrm{Bus(max)}} = 400\ \mathrm{V} \tag{20}$$

$$I_{Q3} = \frac{(1-\delta_{\min})|I_{\mathrm{Bat(max)}}|}{n} = 16\ \mathrm{A} \tag{21}$$

$$I_{Q4} = \frac{\delta_{\max}|I_{\mathrm{Bat(max)}}|}{n} = 10\ \mathrm{A}. \tag{22}$$

B. Power Inductors

Let the peak-to-peak current ripples be 20% of the inductor currents under full power. The current rating and the inductance of the power inductors L_1 and L_2 can be determined using (8)–(11) as follows:

$$I_{\mathrm{L1}} = \delta_{\max} I_{\mathrm{Bat(max)}} = 100\ \mathrm{A} \tag{23}$$

$$I_{L2} = (1-\delta_{\min}) I_{\mathrm{Bat(max)}} = 160\ \mathrm{A} \tag{24}$$

$$L_1 = L_2 = \frac{V_{\mathrm{Bat}} T_s}{0.01\lambda(\%) I_{\mathrm{Bat(max)}}} = 15\ \mu\mathrm{H}. \tag{25}$$

Because of the ripple cancellation on the battery current, a larger ripple current in inductors L_1 and L_2 can be allowed in practical applications. Thus, the inductance and the size of the two inductors L_1 and L_2 might be smaller. The only penalty is the need for two inductors. However, this inconvenience can be partially alleviated by adopting a coupled inductor version.

C. Series Blocking Capacitor

Based on (5), the voltage stress subjected by the series blocking capacitor, C_{s} can be calculated as (26). Practical capacitor voltage rating of 400 V is necessary for safety purposes. The required capacitor magnitude can be determined as (27). The capacitor must, of course, be a film type capacitor with lower ESR

$$V_A = \frac{nV_{\mathrm{Bat}}}{\delta} = 180\ \mathrm{V} \tag{26}$$

$$C_s = \frac{\delta(1-\delta)T_s I_{\mathrm{Bat(max)}}}{0.2nV_A} \approx 10\ \mu F. \tag{27}$$

IV. Simulation and Experimental Verification

To verify the theoretical operating principles, a 2-kW design example was simulated by using IsSpice. Fig. 6 shows the key waveforms in the boost and buck mode operations. There is a good agreement between the simulation results and theoretical analysis. In this research, a 2-kW laboratory prototype was implemented and tested to evaluate the performance of the proposed bidirectional isolated dc–dc converter. Fig. 7(a)–(f) show the measured waveforms in the boost mode operations for the laboratory prototype. The gating signals for the LVS switches

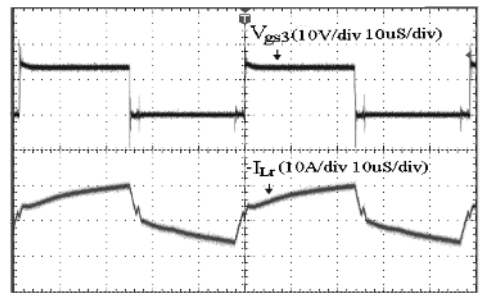

(a)

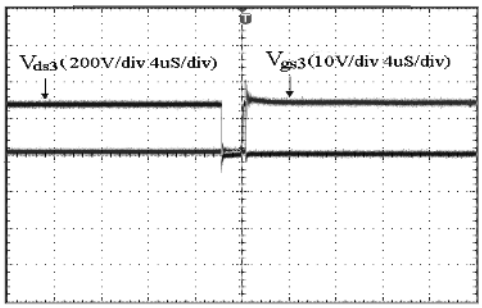

(b)

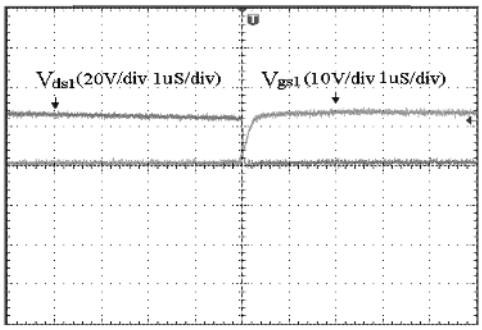

(c)

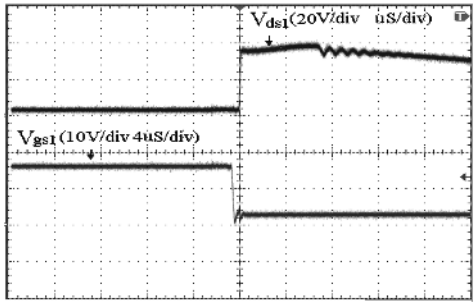

(d)

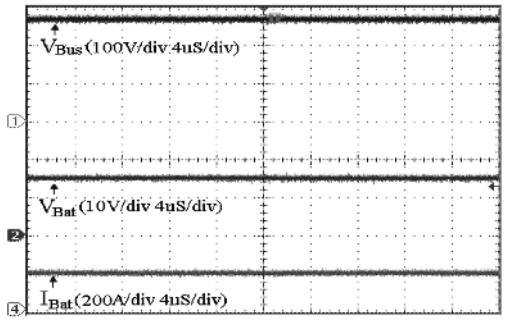

(e)

Fig. 8. Experimental results for buck mode operations for the laboratory prototype.

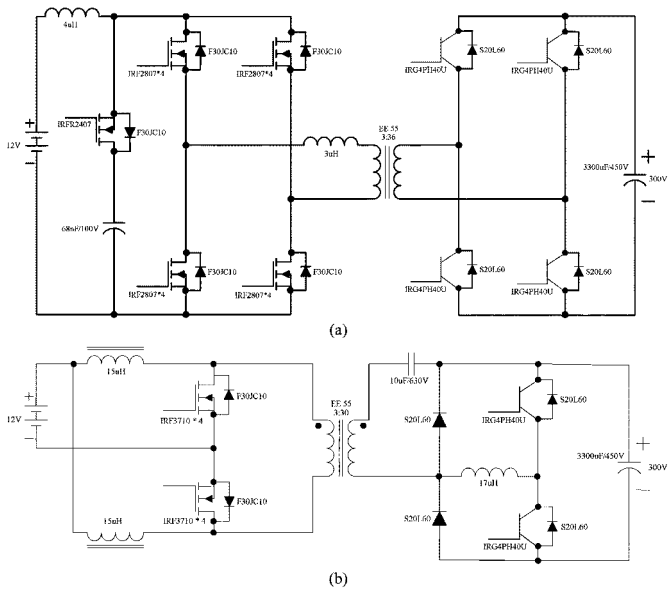

Fig. 9. Schematic diagrams for (a) the conventional and (b) proposed converters.

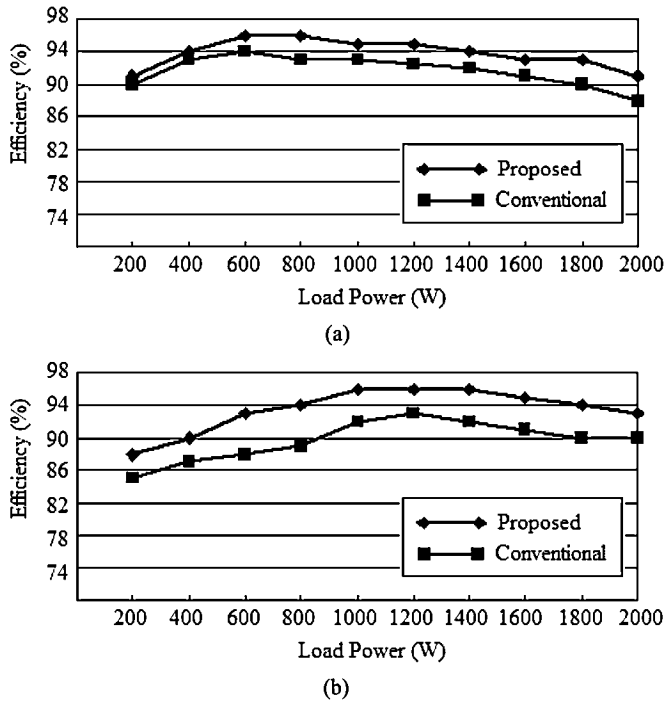

Fig. 10. Efficiency under the load variations in (a) boost, and (b) buck mode operations.

Q1, Q2, and HVS switches Q3, Q4 are shown in Fig. 7(a). The ripple cancellation between two inductor currents can be observed in Fig. 7(b). This is desirable for a low-voltage battery. In Fig. 7(c) and (d), the zero-voltage turn-on details of the HVS switch Q3 and LVS switch Q1 are shown. Fig. 7(e) shows that the peak voltage of V_{ds1} is around 75 V, and the 100-V MOSFET can be used safely. For the conventional full-bridge topology, the peak voltage across the LVS switches is around 45 V, allowing 75-V MOSFET to be used. However, the proposed topology has advantages over the full-bridge topology because of the device count reduction. Fig. 7(f) shows the battery

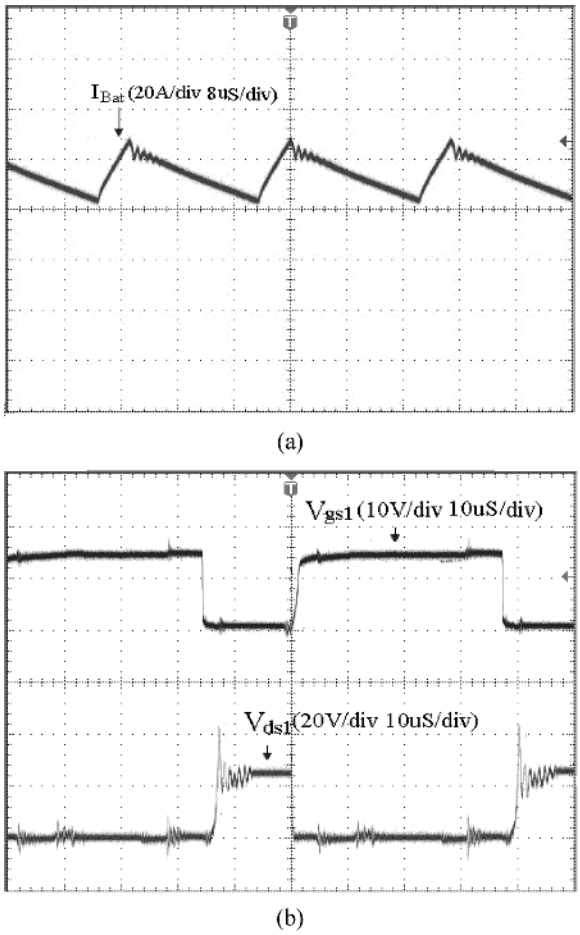

Fig. 11. Test results for the conventional full-bridge topology under boost mode operation.

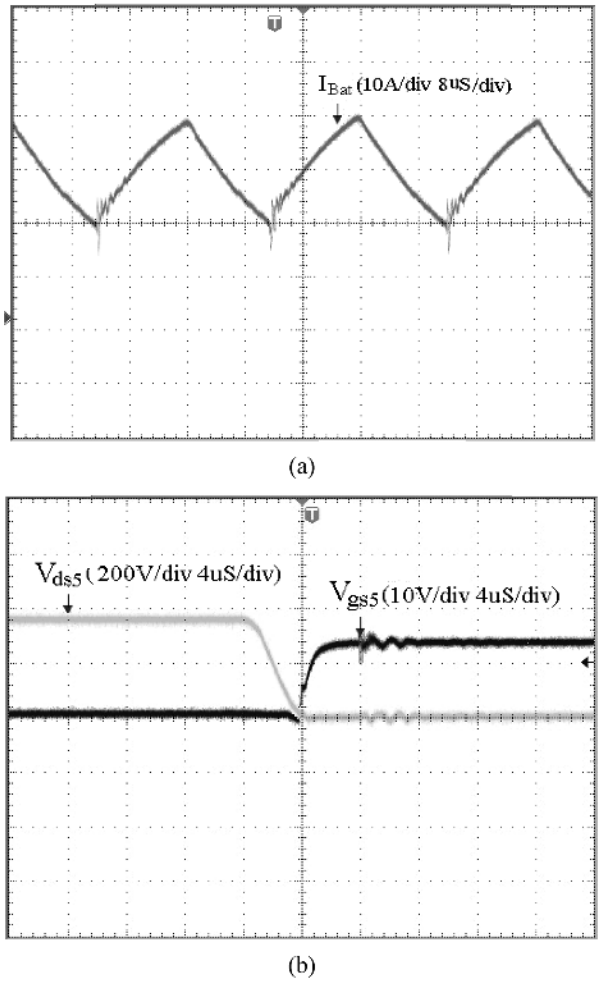

Fig. 12. Test results for the conventional full-bridge topology under buck mode operation.

voltage, $V_{\rm Bat}$, discharging current, $I_{\rm Bat}$, and output voltage on dc bus, $V_{\rm Bus}$. Fig. 8(a)–(e) show the measured waveforms in the buck mode operations for the laboratory prototype. Fig. 8(a) shows the gate signal $V_{\rm gs3}$ for the HVS switch Q3 and resonance inductor current-$I_{\rm Lr}$. The waveforms for illustrating zero-voltage turn-on features of the switches Q1 and Q3 are shown in Fig. 8(b) and (c). Fig. 8(d) shows the measured waveforms of the LVS switch Q1 with zero-voltage turn-off feature. The battery voltage, $V_{\rm Bat}$, charging current, $I_{\rm Bat}$, and output voltage on dc bus, $V_{\rm Bus}$ is shown in Fig. 8(e). The schematic diagrams with detailed circuit parameters for the conventional and proposed converters were shown in Fig. 9(a) and (b) for comparison purposes. Fig. 10(a) and (b) show the efficiency comparisons with the conventional full-bridge converter shown in Fig. 1 under the load variations in the boost and buck mode operations. The proposed converter shows better efficiencies over the entire load range than those of the conventional converter. Because of the device count reduction, higher efficiency can be achieved using the proposed scheme in this paper. Fig. 11 shows the test results for the conventional full-bridge topology under boost mode operation. Fig. 11(a) shows the battery discharging current. The current ripple of the conventional full-bridge topology is obviously higher than that for the proposed topology. As shown in Fig. 11(b), the peak voltage across the LVS switches is around 45 V, allowing a 75-V MOSFET to be used. Fig. 12 shows the circuit operation test results for the full-bridge topology under buck mode operation. Fig. 12(a) shows the battery charging current. The current ripple for the full-bridge topology is higher. In Fig. 12(b), the zero-voltage turn-on details of the HVS switch is shown.

V. Conclusion

A high efficiency bidirectional isolated dc–dc converter for fuel cell electric vehicle driving systems was proposed in this paper. The new converter has the advantages of high efficiency, simple circuit and low cost. The detailed design and operation considerations were analyzed and described. Simulation results from the proposed circuit were given to verify the operation principles. A laboratory prototype was implemented and tested to show its performance.

References

[1] T. E. Lipman, "Manufacturing and lifecycle costs of battery electric vehicles, direct-hydrogen fuel cell vehicles, and direct-methanol fuel cell vehicles," in *Proc. IECEC'00*, 2000, vol. 2, pp. 1352–1358.

[2] K. Rajashekara, "Power conversion and control strategies for fuel cell vehicles," in *Proc. IEEE IECON'03*, 2003, vol. 3, pp. 2865–2870.

[3] Y. Guezennec, T. Y. Choi, G. Paganelli, and G. Rizzoni, "Supervisory control of fuel cell vehicles and its link to overall system efficiency and low-level control requirements," in *Proc. ACC'03*, 2003, vol. 3, pp. 2055–2061.

[4] K. Rajashekara, "Power electronics applications in electric/hybrid vehicles," in *Proc. IEEE IECON'03*, 2003, vol. 3, pp. 3029–3030.
[5] S. Gair, "Motor drives and propulsion systems for EVs," *Proc. Inst. Elect. Eng.*, pp. 3/1–3/6, May 1998.
[6] K. Wang, C. Y. Lin, L. Zhu, D. Qu, F. C. Lee, and J. S. Lai, "Bi-directional dc to dc converters for fuel cell systems," in *Proc. PET'98*, 1998, pp. 47–51.
[7] F. Z. Peng, H. Li, G. J. Su, and J. S. Lawler, "A new ZVS bidirectional dc–dc converter for fuel cell and battery application," *IEEE Trans. Power Electron.*, vol. 19, no. 1, pp. 54–65, Jan. 2004.
[8] G. J. Su, F. Z. Peng, and D. J. Adams, "Experimental evaluation of a soft-switching dc–dc converter for fuel cell applications," in *Proc. PET'02*, 2002, pp. 39–44.
[9] H. Li and F. Z. Peng, "Modeling of a new ZVS Bi-directional dc–dc converter," *IEEE Trans. Aerosp. Electron. Syst.*, vol. 40, no. 1, pp. 272–283, Jan. 2004.
[10] M. Jain, M. Daniele, and P. K. Jain, "A bidirectional dc–dc converter topology for low power application," *IEEE Trans. Power Electron.*, vol. 15, no. 4, pp. 595–606, Jul. 2000.

Huang-Jen Chiu (M'00) was born in I-Lan, Taiwan, R.O.C., in 1971. He received the B.E. and Ph.D. degrees in electronic engineering from National Taiwan University of Science and Technology, Taipei, Taiwan, in 1996 and 2000, respectively.

From August 2000 to July 2002, he was an Assistant Professor in the Department of Electronic Engineering, I-Shou University, Kaohsiung, Taiwan. Since August 2002, he has been with the Department of Electrical Engineering, Chung-Yuan Christian University, Chung-Li, Taiwan, where he is currently an Associate Professor of the Department. His research interests include soft switching techniques, EMC issues, PFC topologies, synchronous rectification, electronic ballast, and DSP control applications.

Dr. Chiu received the Young Researcher Award in 2004 from the National Science Council, R.O.C. He is a member of the IEEE Power Electronics, and Industrial Electronics Societies.

Li-Wei Lin was born in I-Lan, Taiwan, R.O.C., in 1981. He received the B.E. degree in electrical engineering from Ming-Hsin University of Science and Technology, Hsinchu, Taiwan, in 2003 and is currently pursuing the Ph.D. degree in the Department of Electrical Engineering, Chung-Yuan Christian University, Chung-Li, Taiwan.

His research interests include soft switching techniques, synchronous rectification, PWM inverters, and control applications.